



# Performance Analysis of OFDM With Peak Cancellation Under EVM and ACLR Restrictions

Tomoya Kageyama , *Student Member, IEEE*, Osamu Muta , *Member, IEEE*,  
and Haris Gacanin , *Senior Member, IEEE*

**Abstract**—This paper presents performance analysis of an adaptive peak cancellation (PC) method to reduce the high peak-to-average power ratio (PAPR) for OFDM systems, while keeping the out-of-band (OoB) power leakage as well as an in-band distortion power below the pre-determined level. In this work, the increase of adjacent leakage power ratio (ACLR) and error vector magnitude (EVM) are estimated recursively using the detected peak amplitude. We present analytical framework for OFDM-based systems with theoretical bit error rate (BER) representations and detection of optimum peak threshold based on predefined EVM and ACLR requirements. Moreover, the optimum peak detection threshold is selected based on theoretical design to maintain the pre-defined distortion level. Thus, their degradations are restricted below the pre-defined levels which correspond to target OoB radiation. We also discuss the practical design of peak-cancellation signal with target OoB radiation and in-band distortion through optimizing the windowing size of the PC signal. Numerical results show the improvements with respect to both achievable BER and PAPR with the PC method in eigen-beam space division multiplexing (E-SDM) systems under restriction of OoB power radiation. It can also be seen that the theoretical BER shows good agreements with simulation results.

**Index Terms**—PAPR, ACLR, EVM, OoB radiation, OFDM.

## I. INTRODUCTION

**F**UTURE wireless communication systems require robust communication over a frequency-selective fading channel [1], such as orthogonal frequency division multiplexing (OFDM) with multi-input multi-output (MIMO) technologies. One of the technical issues in MIMO-OFDM is the reduction of peak-to-average power ratio (PAPR).

Manuscript received September 15, 2019; revised January 17, 2020; accepted March 3, 2020. Date of publication April 2, 2020; date of current version June 18, 2020. This work was supported in part by Japan Society for the Promotion of Science (JSPS) KAKENHI under Grants JP17K06427 and JP17J04710, and in part by Kyushu University Short-term International Research Exchange Program by University Research Administration Office. This work was presented in part at the 2015 IEEE International Symposium on Personal Indoor and Mobile Radio Communication (IEEE PIMRC 2015) [31]. The review of this article was coordinated by Dr. V. Marojevic. (*Corresponding author: Tomoya Kageyama.*)

Tomoya Kageyama is with the Graduate School of Information Science and Electrical Engineering, Kyushu University in Japan, Fukuoka 812-8581, Japan (e-mail: kageyama@mobcom.ait.kyushu-u.ac.jp).

Osamu Muta is with the Center for Japan-Egypt Cooperation in Science and Technology, Kyushu University in Japan, Fukuoka 812-8581, Japan (e-mail: muta@ait.kyushu-u.ac.jp).

Haris Gacanin is with the RWTH Aachen University in Germany, Aachen 52062, Germany (e-mail: harisg@ieee.org).

Digital Object Identifier 10.1109/TVT.2020.2982587

Existing PAPR reduction techniques can be categorized into probabilistic-based approach [3]–[13], coding-based [14]–[16], and limiter (deliberate clipping) [17]–[32]. Contemporary communication systems rely on a simple PAPR reduction technique without any additional processing at the receiver end. Deliberate clipping and filtering (C&F) [17]–[24] is an attractive technique from the viewpoint of its simple implementation, but it introduces nonlinear degradations. In C&F, filtering is used to remove OoB radiation, but it causes the re-growth of signal amplitude after filtering. Other related approaches such as peak windowing, peak cancellation (PC), and companding (e.g., [25]–[32]) have also been investigated. In principle, C&F and its simplified versions produce nonlinear distortion that may be measured by using error vector magnitude (EVM) and adjacent channel leakage power ratio (ACLR). To cope with them, initial studies of peak cancellation under out-of-band radiation has been presented in [30], [31]. However, in these works, the peak detection threshold level is empirically determined and also the optimum peak detection threshold and bit error rate (BER) analysis are not theoretically given. From the practical system design point of view, they should be kept below a pre-defined optimum threshold. An analytical evaluation of their impacts on transmission system design is an important study item. This is even more important since the BER performance of the pre-coded OFDM system is highly sensitive to nonlinear degradations. Main contributions are as follows.

- We present an adaptive peak cancellation method to keep EVM and ACLR below permissible level for multi-input multi-output (MIMO)-OFDM system. In this method, an amplitude that exceeds a given threshold is suppressed repeatedly by efficient design of PC signal, while optimizing the system performance for pre-defined ACLR and EVM. The proposed method is an efficient distortion estimator for linearly pre-coded MIMO-OFDM, where the increases of ACLR and EVM are estimated recursively using the detected peak amplitude, respectively.
- Unlike the peak cancellation in [31], we present an analytical framework for OFDM-based systems with detection of optimum peak threshold (i.e., theoretically achieved PAPR lower bound) based on EVM and ACLR. In this framework, the optimum peak detection threshold is selected based on the analytical results to achieve the pre-defined distortion level.
- We develop an analytical framework for single antenna and multi-antenna systems, respectively. Our analysis confirms

that signal distortion due to the peak cancellation is a random variable which follows Gaussian distribution whose variance and average power is determined based on the optimum peak detection threshold.

- We discuss about practical design of peak cancellation signal, where achievable OoB radiation and in-band distortion can be adjusted by optimizing the windowing size of the PC signal. We evaluate the achievable performance of our proposed method in terms of BER, complementary cumulative distribution function (CCDF) of PAPR as well as computational complexity in pre-coded MIMO-OFDM systems using eigenbeam space division multiplexing (E-SDM). The proposed method is able to restrict ACLR and EVM below their permissible levels without empirically determining the parameters such as the number of PC signal additions. The results show that the proposed method achieves lower peak power and computational complexity compared to the case of repeated C&F under the restriction of OoB power radiation.

## II. RELATED WORKS

Limiter based PAPR reduction techniques have been investigated for OFDM systems in the literature. In particular, various C&F based approaches are presented such as in [20]–[32]. In [20], an adaptive selection method of peak detection threshold is proposed to achieve fast convergence in repeated C&F. This method is effective in reducing the required number of iterations in C&F. However, in-band distortion due to clipping is not restricted below a pre-defined level. In [21], an optimized filtering method is proposed for repeated C&F in which filter characteristic is optimized to minimize in-band distortion (i.e., EVM) under PAPR constraint while limiting the OoB radiation. Using this method, the required number of repetitions is reduced compared with traditional repeated C&F. In [22], a modified repeated C&F method is presented, where the clipped signal is optimized by minimizing the increase of in-band distortion at each clipping iteration under PAPR constraint. This method is also effective in reducing the required number of iterations in repeated C&F. However, the above methods still require repeated filtering operations to limit OoB radiation which results in increased computational complexity. In [23], a simplified C&F technique using a neural network is proposed. In this method, band-limited clipped signal is approximately generated with a learning-based approach without actual filtering process. Thus, the required complexity to reduce PAPR is reduced. However, the bit error rate is degraded due to inaccurate approximation as modulation order increases. Thus, more complicated learning method may be needed for signals with higher-order modulation. In [24], a repeated C&F method that adaptively determines the clipping threshold is proposed. Although this method does not require a pre-defined threshold, in-band distortion is not restricted below a pre-defined level. In [32], a new limiter based companding function was proposed to suppress peak amplitude effectively. However, companding transformation causes OoB radiation due to nonlinearity of companding function.

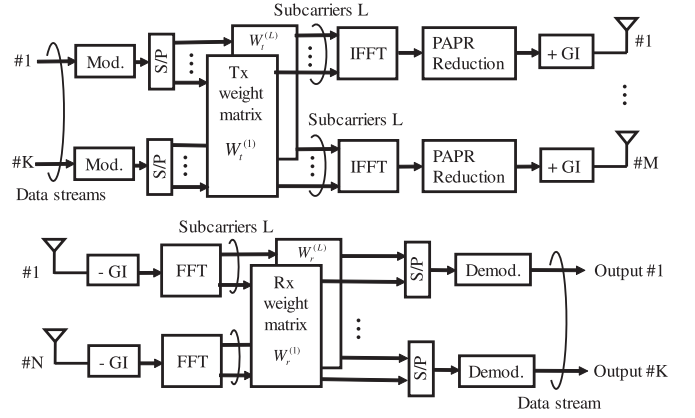


Fig. 1. System block diagram.

Unlike the above approaches, in this paper, we designed an effective peak cancellation method that restricts EVM and ACLR below the optimum pre-defined level, while reducing the peak amplitude below the threshold level with lower complexity than the conventional repeated C&F.

## III. MATHEMATICAL SIGNAL REPRESENTATION

### A. System Model

Fig. 1 illustrates an E-SDM OFDM system model, where  $M$ ,  $N$ , and  $K$  denote the number of transmit antennas, receive antennas, and data streams, respectively.  $\mathbf{W}_t^l$  and  $\mathbf{W}_r^l$  denote precoding and post-coding matrices on the  $l$ -th subcarrier, respectively, where  $l = 1, \dots, L$ , and  $L$  denotes the number of subcarriers. Here, the transmit data vector of the  $l$ -th subcarrier  $\mathbf{x}^l = [x_1^l, \dots, x_k^l, \dots, x_K^l]^T$  is multiplexed by the precoding matrix  $\mathbf{W}_t^l = [\mathbf{w}_{t1}^l, \dots, \mathbf{w}_{tk}^l, \dots, \mathbf{w}_{tK}^l]$ , where  $\mathbf{w}_{tk}^l = [w_{tk1}^l, \dots, w_{tkm}^l, \dots, w_{tkM}^l]^T$  is the  $l$ -th column vector of  $\mathbf{W}_t^l$  for the  $k$ -th data stream and superscript  $T$  stands for transposed matrix. In E-SDM, left singular vector and right singular vector of the channel matrix are used as precoding and post-coding matrices, respectively.  $\mathbf{H}^l$  stands for  $N \times M$  matrix of the  $l$ -th subcarrier defined as

$$\mathbf{H}^l = \begin{pmatrix} h_{11}^l & \dots & h_{1M}^l \\ \vdots & h_{nm}^l & \vdots \\ h_{N1}^l & \dots & h_{NM}^l \end{pmatrix}, \quad (1)$$

where  $h_{nm}^l$  denotes impulse response of the path. Here, the  $m$  and  $n$  denote the transmit antenna index and the receive antenna index, respectively. Using with singular value decomposition (SVD),  $\mathbf{H}^l$  can be decomposed into

$$\mathbf{H}^l = \mathbf{U}_l \Sigma_l \mathbf{V}_l^H, \quad (2)$$

where  $\mathbf{U}_l$  and  $\mathbf{V}_l^H$  are left and right singular vector of  $\mathbf{H}^l$ , and  $(\cdot)^H$  means complex conjugate operation.  $\Sigma_l = \text{diag}(\sqrt{\lambda_1^l}, \sqrt{\lambda_2^l}, \dots, \sqrt{\lambda_M^l})$  is a diagonal matrix and  $\sqrt{\lambda_m^l}$  is the singular value of  $m$ -th stream. Transmit and receive spatial filter are defined as  $\mathbf{W}_t^l = \mathbf{V}_l$  and  $\mathbf{W}_r^l = \mathbf{U}_l^H$ . The pre-coded

QAM data stream is modulated with inverse fast Fourier transform (IFFT) and then PAPR reduction technique is applied at each transmits antenna. The guard interval (GI) is added to every symbol to remove inter-symbol interference. Perfect channel estimation is assumed.

After removing GI and carrying out FFT processing, the received signal is multiplied by the post coding matrix  $\mathbf{W}_r^l = [\mathbf{w}_{r1}^l, \dots, \mathbf{w}_{rk}^l, \dots, \mathbf{w}_{rK}^l]^T$ , where  $\mathbf{w}_{rn}^l = [w_{rn1}^l, \dots, w_{rnk}^l, \dots, w_{rnK}^l]^T$  denotes the  $n$ -th post-coding vector of the  $l$ -th subcarrier. The received signal vector after passing through the received filter is  $\mathbf{y}^l = [y_1^l, \dots, y_k^l, \dots, y_K^l]^T$  given as

$$\begin{aligned} \mathbf{y}^l &= \mathbf{W}_r^l (\mathbf{H}^l \mathbf{W}_i^l \mathbf{x}^l + \mathbf{n}^l) \\ &= \mathbf{U}_i^H (\mathbf{H}^l \mathbf{V}_i \mathbf{x}^l + \mathbf{n}^l) \\ &= \mathbf{U}_i^H (\mathbf{U}_i \Sigma_i \mathbf{V}_i^H \mathbf{V}_i \mathbf{x}^l + \mathbf{n}^l) \\ &= \Sigma_i \mathbf{x}^l + \mathbf{U}_i^H \mathbf{n}^l, \end{aligned} \quad (3)$$

where  $\mathbf{U}_i$  and  $\mathbf{V}_i$  are unitary matrices and  $\mathbf{n}^l = [n_1, \dots, n_n, \dots, n_N]^T$  is an additive white Gaussian noise (AWGN) vector at each receive antenna.

### B. Definitions of ACLR and EVM

In this paper, we evaluate the amount of OoB radiations as ACLR which is defined as

$$\text{ACLR} = \int_{f_U, f_L} \frac{S(\omega)}{S_t} d\omega. \quad (4)$$

Here,  $S_t = \frac{1}{2} E[|x_k^l|^2]$  denotes the average power of the transmit signal and  $S(\omega)$  is the power spectral density of the transmitted signal.

Let  $f_U$  and  $f_L$  denote the measured ACLR at an upper and lower band, respectively. The permissible maximum ACLR is set to  $-50$  dB for transmitting signals at every antennas.

We also evaluate in-band distortion by measuring EVM which is defined as:

$$\text{EVM} = \sum_{l=-L/2+1}^{L/2} |X_l - \tilde{X}_l|^2 / \sum_{l=-L/2+1}^{L/2} S_t[l], \quad (5)$$

where  $S_t[l]$  is the average power of the  $l$ -th subcarrier signal.  $X_l$  and  $\tilde{X}_l$  denote the complex signals at the  $l$ -th subcarrier (after FFT operation) without and with PAPR reduction, respectively. In E-SDM case,  $X_l$  and  $\tilde{X}_l$  are defined as complex signals and replicated at the  $l$ -th subcarrier of each eigen-channel by Eq. (3).

## IV. ADAPTIVE PEAK-CANCELLATION TECHNIQUE

Fig. 2(a) shows the block diagram of our designed peak cancellation which consists of five steps, i.e., PC signal generation, selection of the peak detection threshold, peak detector, distortion estimation, and PC signal scaling, where  $x^{(m,i)}(t)$  denotes input signal at  $m$ -th antenna at  $i$ -th repetition.

The first two blocks ("PC signal generation" and "selection of the peak detection threshold") are carried out beforehand. In each transmission frame, whenever the maximum amplitude  $x_{max}^{(m,i)}$  exceeding the threshold  $A_{th}$  is detected at the peak

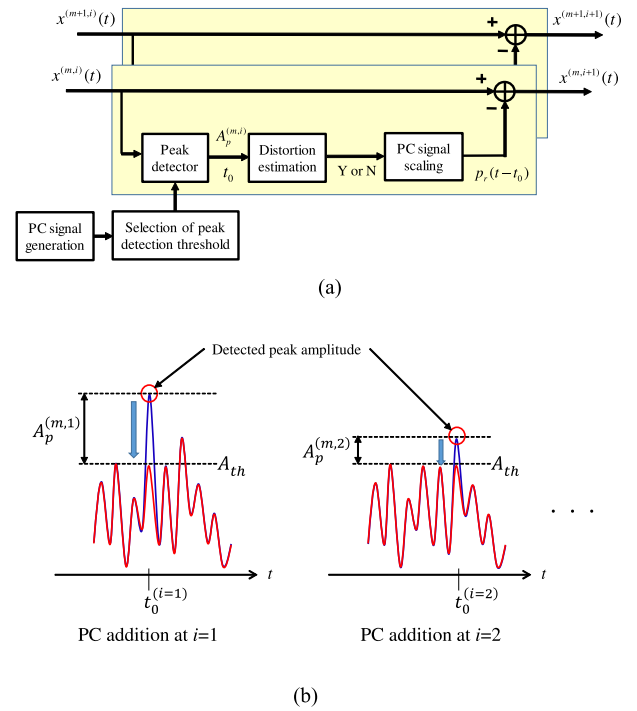


Fig. 2. The concept of the proposed method. (a) Block diagram of the proposed method, where  $x^{(m)}(t, i)$  denotes the transmit signal at  $m$ -th antenna after adding  $i$ -th PC signal. (b) Peak cancellation process at  $m$ -th antenna.

detector, the distortion estimation is carried out using a recursive method, and it decides whether both the maximum ACLR and an average EVM over all antennas are kept below their given values or not (i.e., binary decision; "Y" or "N").

If the estimated values are below the pre-defined values, the amplitude of the PC signal is scaled to  $A_p^{(m,i)} = |x_{max}^{(m,i)}| - A_{th}$ .

Then, the scaled PC signal is added to reduce  $|x_{max}^{(m,i)}|$  to  $A_{th}$ . Otherwise, the peak cancellation procedure stops. The details of each step are explained below.

*Step 1: Peak Cancellation Signal Generation:* Whenever the maximum signal amplitude exceeds a given threshold level  $A_{th}$ , the maximum peak is suppressed by adding a PC signal. Here, the PC signal is a scaled OFDM symbol whose subcarriers are added up to be in-phase at a given symbol time instant. The PC signal is generated by scaling the following basic function  $g(t)$  as

$$g(t) = \frac{1}{L} \sum_{l=-L/2+1}^{L/2} p_l(t) e^{j\omega_l t}, \quad (6)$$

where  $p_l(t)$  is the transmit pulse at the  $l$ -th subcarrier. In this paper, we assume that  $p_l(t)$  is the same rectangular pulse on all subcarriers whose amplitude is unity. The time-domain waveform of  $g(t)$  is truncated by a windowing function  $w(t)$ ; the truncated version of  $g(t)$  is given as

$$g'(t) = w(t)g(t). \quad (7)$$

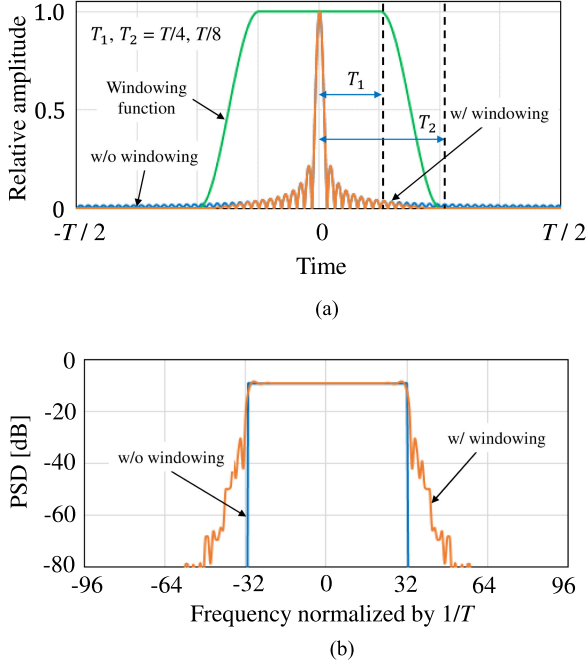


Fig. 3. An example of peak cancellation (PC) signal. (a) Time-domain waveform. (b) Frequency-domain spectrum.

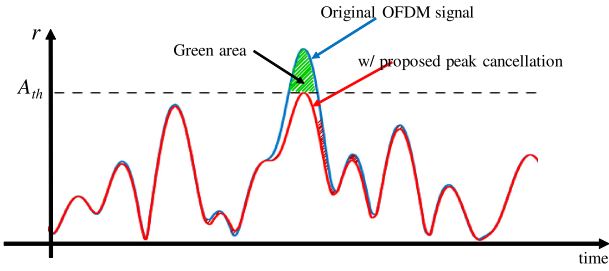


Fig. 4. Illustration of the peak cancellation effect.

We use the following windowing function to truncate the peak cancellation signal waveform:

$$w(t) = \begin{cases} 0 & (T_2 < |t|) \\ \frac{1}{2} + \frac{1}{2} \cos \frac{\pi(|t|-T_1)}{T_2-T_1} & (T_1 < |t| \leq T_2) \\ 1 & (|t| \leq T_1), \end{cases} \quad (8)$$

where  $0 < T_1 \leq T_2$ . Here,  $T_1$  is a design parameter to optimize distortions appeared after peak cancellation.  $T_2$  denotes window size of  $w(t)$ . The truncated PC signal waveform and its frequency spectrum of  $g'(t)$  are illustrated in Fig. 3(a) and (b), respectively. Here, parameters of windowing function are given as  $(T_1, T_2) = (T/8, T/4)$ , where  $T$  is a symbol duration. The PC signal explicitly exhibits high peak amplitude which is utilized to reduce the PAPR of OFDM.

**Step 2: Selection of Peak Detection Threshold:** In the proposed method, the optimum peak detection threshold should be selected so that the signal amplitude is suppressed below the threshold level, while EVM and ACLR are kept below the predefined values. This subsection describes the optimum threshold selection. Fig. 4 illustrates an example of an OFDM signal waveform. In this figure, red and blue lines show the signal with and without the proposed peak cancellation, respectively. The

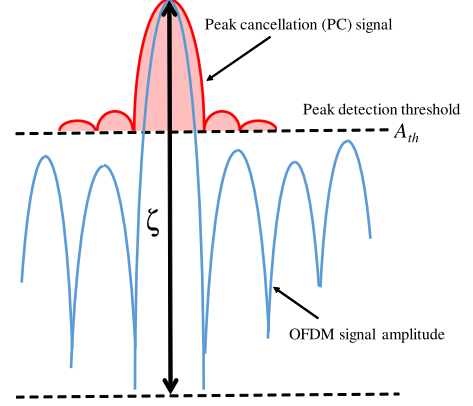


Fig. 5. Modeling of signal distortion due to PC signal addition.

green-shaded area corresponds to signal amplitude exceeding the peak detection threshold  $A_{th}$ . As illustrated in Fig. 4, adding the PC signal distorts the OFDM signal and increases both EVM and ACLR.

Fig. 5 illustrates the relation between the scaling factor of the PC signal and the peak detection threshold, where  $\zeta$  and  $A_{th}$  denote the maximum amplitude of the OFDM signal and the peak detection threshold, respectively. As illustrated in Fig. 5, when the maximum amplitude  $\zeta$  exceeds the threshold level  $A_{th}$ , OFDM signal amplitude is reduced to the threshold level by adding the PC signal whose amplitude is scaled to  $\zeta - A_{th}$ . Since the scaled PC signal is given as  $(\zeta - A_{th})g'(t)$ , the energy of the scaled PC signal is calculated as

$$\begin{aligned} E(\zeta - A_{th}) &= \int_{-T_2}^{T_2} (\zeta - A_{th})^2 g'^2(t) dt \\ &= (\zeta - A_{th})^2 \int_{-\infty}^{\infty} G'^2(\omega) d\omega \\ &= (\zeta - A_{th})^2 \left( \int_{f_{in}} G'^2(\omega) d\omega + \int_{f_{out}} G'^2(\omega) d\omega \right) \\ &\equiv (\zeta - A_{th})^2 (E_i + E_o), \end{aligned} \quad (9)$$

where  $f_{in}$  and  $f_{out}$  denote bandwidths to measure EVM and ACLR, respectively. Here,  $G'(\omega) = \int_{-\infty}^{\infty} g'(t)e^{-j\omega t} dt$ .  $E_i$  and  $E_o$  denote in-band power and out-of-band power of PC signal, respectively. Statistical distribution of instantaneous power of the OFDM signal follows exponential distribution as

$$r(\zeta) = \frac{1}{\sigma^2} \exp\left(-\frac{\zeta^2}{\sigma^2}\right), \quad (10)$$

where  $\zeta^2$  and  $S_t = \sigma^2$  denotes instantaneous power and average power of OFDM signal, respectively. Thus, the average signal distortion due to peak cancellation is calculated as

$$\begin{aligned} S_d &= \int_{A_{th}}^{\infty} E(\zeta - A_{th}) r(\zeta) d\zeta \\ &= (E_i + E_o) \int_{A_{th}}^{\infty} (\zeta - A_{th})^2 r(\zeta) d\zeta. \end{aligned} \quad (11)$$

The in-band distortion power is given as

$$S_{in} = E_i \int_{A_{th}}^{\infty} (\zeta - A_{th})^2 r(\zeta) d\zeta. \quad (12)$$

Assuming  $E_i \gg E_o$ , the normalized signal distortion is restricted as

$$\frac{S_d}{S_t} \approx \frac{S_{in}}{\sigma^2} \leq \frac{e_r}{\sigma^2}, \quad (13)$$

where the average power of the signal is  $S_t = \sigma^2$  and  $\frac{e_r}{\sigma^2}$  denotes the pre-determined value of the maximum acceptable EVM. Hence, the minimum (optimum) peak detection threshold  $A_{th}^o$  that meets the EVM requirement is given as

$$\int_{A_{th}^o}^{\infty} (\zeta - A_{th}^o)^2 r(\zeta) d\zeta = \frac{e_r}{E_i}. \quad (14)$$

Here,  $(A_{th}^o)^2$  corresponds to the peak power of the OFDM signal after peak cancellation. Using Eq.(14), the optimum threshold  $A_{th}^o$  to achieve pre-determined EVM value can be theoretically obtained.

*Step 3: Peak Detection and the Remaining Processing:* As in Fig. 2(a), the remaining three steps (i.e., “peak detection,” “distortion estimation,” and “PC signal scaling”) are repeated until the peak amplitude is below the threshold value unless the estimated distortion (i.e., ACLR or EVM) exceeds their pre-defined values. More concretely, as illustrated in 2(b), at the first iteration ( $i=1$ ), if the peak amplitude of OFDM signal at  $m$ -th antenna exceeds the selected peak detection threshold at time instance  $t = t_0^{(m,i)}$ , the difference between the detected peak amplitude and the detection threshold,  $A_p^{(m,i)}$ , is calculated by adding the PC signal. Similarly, at the 2nd iteration ( $i = 2$ ), if the peak amplitude exceeds the threshold, PC signal is added again to cancel this peak amplitude. The increase of ACLR and EVM is estimated using the detected value  $A_p^{(m,i)}$ . Details of distortion estimation and peak cancellation are explained in Steps 4 and 5.

*Step 4: Distortion Estimation:* In multi-stream transmission in MIMO-OFDM, the peak cancellation is carried out to suppress the peak amplitude below the peak detection threshold under constraints of EVM and ACLR, where EVM and ACLR requirements are defined as an average value and the maximum value over all antennas, respectively.

Since the truncated signal  $g'[s] = g'(s\Delta t)$  has out-of-band spectrum, it is clear that out-of-band radiation and in-band distortion appears by adding  $g'[s]$  to the transmit signal, where  $\Delta t$  denotes sampling interval. Here,

$$G'[l] = \mathcal{F}[g'[s]] = W[l]*G[l],$$

where  $\mathcal{F}$  and  $*$  denote discrete Fourier transform and convolution operator, respectively.  $G[l]$  and  $W[l]$  are frequency spectrum of the PC signal  $g[s]$  and the window function  $w[s]$ , respectively.

Let  $\Delta p_o$  and  $\Delta p_{in}$  denote OoB signal power and in-band signal power of  $g'(t)$ . Note that  $\Delta p_o$  and  $\Delta p_{in}$  are known values (calculated beforehand). Hence, when  $G'[l]$  is added to the signal

to cancel the peak, the in-band distortion and OoB radiation are increased by

$$\begin{cases} \Delta p_{in} = \sum_{l=-L/2}^{L/2} |G'[l]|^2, \\ \Delta p_o = \sum_{l=L/2+2}^{3L/2+1} |G'[l]|^2 + \sum_{l=-3L/2}^{-(L+2)/2} |G'[l]|^2. \end{cases} \quad (15)$$

Let the total transmission power  $S_t$  be constant, i.e.,  $S_t = \sum_{m=1}^M S^{(m)}$ , where  $S^{(m)}$  is the average signal power at the  $m$ -th transmit antenna. Let  $|A_p^{(m,i)}|$  denote the difference between the threshold value and the  $i$ -th peak amplitude  $x_{max}^{(i)}$  at the  $m$ -th antenna. EVM increase is expressed as  $\frac{1}{S_t} |A_p^{(m,i)}|^2 \Delta p_{in}$  when the PC signal is added to suppress the  $i$ -th peak amplitude  $x_{max}^{(i)}$ .

We calculate an average EVM value overall antennas as

$$\Delta \varepsilon_e^{(i)} = \sum_{m=1}^M \frac{1}{S_t} |A_p^{(m,i)}|^2 \Delta p_{in} = \frac{\Delta p_{in}}{S_t} \sum_{m=1}^M |A_p^{(m,i)}|^2, \quad (16)$$

where  $\Delta p_{in}$  denotes the pre-determined constant. The averaged EVM value  $\varepsilon_e^{(i)}$  is recursively calculated as

$$\varepsilon_e^{(i)} = \varepsilon_e^{(i-1)} + \Delta \varepsilon_e^{(i-1)}. \quad (17)$$

In order to restrict OoB radiation below the permissible value, we propose to estimate the instantaneous ACLR at each antenna as follows: The estimated ACLR at the  $i$ -th iteration can be estimated as the following recursive equation.

$$\Delta \varepsilon_a^{(m,i)} = \frac{\Delta p_o}{S_t/M} |A_p^{(m,i)}|^2, \quad (18)$$

where  $S_t/M$  denotes the transmit signal power per antenna. The second term of the right-hand side means how much ACLR is increased at the  $i$ -th PC signal addition. The worst (i.e., maximum) ACLR among all antennas is calculated as

$$\varepsilon_a^{(i)}_{max} = f(\varepsilon_a^{(m,i)})_{max:m}, \quad (19)$$

where  $f(\cdot)_{max:m}$  is a function that selects the maximum value from possible ones with respect to antenna index  $m$ . The proposed method cancels the peak amplitude unless the estimated worst ACLR among all antennas exceeds the permissible level. In other words, in the proposed method, the worst ACLR can be restricted below the permissible one.

The PC signal scaling and peak cancellation procedure in next step is done if both the average EVM  $\varepsilon_e^{(i)}$  in Eq. (17) and the maximum ACLR  $\varepsilon_a^{(i)}_{max}$  in Eq. (19) are less than the pre-defined levels.

*Step 5: PC Signal Scaling and Peak Cancellation:* The PC signal is added so that the peak signal amplitude is reduced to  $A_{th}$  while  $\varepsilon_a^{(i)}_{max}$  and  $\varepsilon_e^{(i)}$  satisfy the permissible values. When the OFDM signal amplitude  $x^{(m,i)}(t_0^{(m,i)})$  exceeds the threshold, the scaled PC signal is expressed as

$$lp_r^{(m,i)}(t - t_0^{(m,i)}) = -A_p^{(m,i)} e^{j\theta_0^{(m,i)}} g'(t - t_0^{(m,i)}), \quad (20)$$

where  $A_p^{(m,i)} = |x^{(m,i)}(t_0^{(m,i)})| - A_{th}$ ,  $\theta_0^{(m,i)}$  is phase of the signal  $x(t_0^{(m,i)})$ , i.e.,  $x(t_0^{(m,i)}) = |x(t_0^{(m,i)})| e^{j\theta_0^{(m,i)}}$ . Since the PC signal has an opposite phase of OFDM signal at  $t = t_0^{(m,i)}$ ,

it is guaranteed that the peak amplitude can be reduced to the threshold level. Although the signal amplitude may fluctuate by adding PC signals, all peak amplitudes can be suppressed below the threshold level by repeating the above process (i.e. adding PC signals iteratively). Then, As illustrated in Fig. 2(b), the amplitude of OFDM signal at  $t = t_0^{(m,i)}$  is reduced to the threshold value as shown below:

$$x^{(m,i)}(t) = x^{(m,i-1)}(t) + p_r^{(m,i)}(t - t_0^{(m,i)}), \quad (21)$$

where  $x^{(m,i)}(t)$  is the transmit signal after canceling the  $i$ -th peak amplitude by adding the PC signal,  $p_r^{(m,i)}(t - t_0^{(m,i)})$ . The above repetition are continued until all peak amplitudes that exceed the threshold  $A_{th}$  are suppressed or the estimated ACLR or EVM reach a given pre-defined value. In other words, the proposed method guarantees that both EVM and ACLR meet their requirements without empirically determining the number of PC signal additions.

## V. BER ANALYSIS OF OFDM WITH THE DESIGNED PEAK CANCELLATION

In this section, we analyze theoretical BERs of single antenna OFDM and linearly pre-coded (E-SDM) MIMO-OFDM with our designed peak cancellation, respectively.

### A. Single Antenna OFDM

In this section, first, we consider QPSK-OFDM signal whose subcarrier's I and Q-phases take either  $A$  or  $-A$ . Let  $x_e$  denote a random variable which expresses signal distortion due to peak cancellation. Thus, the signal after peak cancellation is given as  $\pm A + x_e$ . We assume that  $x_e$  follows Gaussian distribution with variance  $\sigma_e^2$  and average value  $\bar{x}_e$ ;

$$p_e(x_e) = \frac{1}{\sqrt{2\pi\sigma_e^2}} \exp\left(-\frac{(x_e - \bar{x}_e)^2}{2\sigma_e^2}\right), \quad (22)$$

where  $\sigma_e^2$  and  $\bar{x}_e$  are variance and average amplitude of  $x_e$ . Since the average power of the signal is decreased after peak cancellation, it can be intuitively seen that  $\bar{x}_e$  decreases as  $A_{th}$  decreases, while  $\sigma_e$  increase as  $A_{th}$  decreases. Hence, the average value of  $x_e$  can be expressed with  $S_{in}$  as

$$\bar{x}_e \approx -\alpha\sqrt{S_{in}/L}, \quad (23)$$

where  $L$  denotes the number of subcarriers.  $\alpha$  is a constant depending on PC signal waveform  $g'(t)$  given as

$$\alpha = \frac{\int_{-\infty}^{\infty} f_c(\text{Re}[g'(t)])dt}{\int_{-\infty}^{\infty} |\text{Re}[g'(t)]|dt}. \quad (24)$$

where  $f_c(x)$  denotes a clipping function defined as

$$f_c(x) = \begin{cases} x & x > 0 \\ 0 & \text{otherwise.} \end{cases} \quad (25)$$

The numerator and the denominator in Eq.(24) show integral of positive side PC signal amplitude and that of its absolute value, respectively. The variance of  $x_e$  is given as

$$\sigma_e^2 = \langle (A + x_e - \mu A)^2 \rangle = \mu^2(S_{in}/L),$$

where  $\mu = 1 - \bar{x}_e/A$ . Here,  $\langle x \rangle$  denotes expected value of the variable  $x$ .

Let  $x_n$  denote additive white Gaussian noise (AWGN) with average level  $A$  and variance  $\sigma_n^2$ , i.e., PDF of  $x_n$  is given as

$$p_n(x_n, \sigma_n) = \frac{1}{\sqrt{2\pi\sigma_n^2}} \exp\left(-\frac{x_n^2}{2\sigma_n^2}\right), \quad (26)$$

$x_e$  and  $x_n$  are Independent and identically distributed (i.i.d.) random variables and therefore PDF of mixed variable  $x = x_e + x_n$  is given as convolution of  $p_x(x)$  and  $p_n(x)$ :

$$\begin{aligned} p(x, \sigma_n, \sigma_e, \beta) &= \int_{-\infty}^{\infty} p_e(x - y, \sigma_e, \beta) p_n(y, \sigma_n) dy \\ &= \frac{1}{\sqrt{2\pi((\sigma_e^2/\beta) + \sigma_n^2)}} \exp\left(-\frac{(x - (\bar{x}_e/\sqrt{\beta}))^2}{2((\sigma_e^2/\beta) + \sigma_n^2)}\right), \end{aligned}$$

where  $\beta$  denotes channel gain. BER for QPSK-OFDM signal after peak cancellation in AWGN condition with channel gain is expressed as

$$\begin{aligned} P_b(A, \sigma_n, \sigma_e, \beta) &= \int_{-\infty}^0 p(x - A, \sigma_n, \sigma_e, \beta) dx \\ &= \int_0^{\infty} \frac{1}{\sqrt{2\pi((\sigma_e^2/\beta) + \sigma_n^2)}} \exp\left(-\frac{(x - (\bar{x}_e/\sqrt{\beta}))^2}{2((\sigma_e^2/\beta) + \sigma_n^2)}\right) dx, \end{aligned} \quad (27)$$

where  $A$  denotes I and Q phase signal amplitudes.

The above discussion can be extended to multi-level QAM such as 16QAM and 64QAM. The same manner as QPSK case can be used for deriving BER expressions in QAM case except that variance of in-band noise is different, e.g., for 16QAM and 64QAM cases, their variances  $\sigma_e^{16QAM}$  and  $\sigma_e^{64QAM}$  are respectively given as

$$\sigma_e^{16QAM} = \sigma_e/2, \quad (28)$$

$$\sigma_e^{64QAM} = \sigma_e/4, \quad (29)$$

where  $\sigma_e$  denotes variance in QPSK case. More generally, variance for  $2^Q$  QAM is given as  $\sigma_e/Q$

Fig. 6 shows I-phase or Q-phase signal distribution of 16QAM at a certain subcarrier in the case with and without peak cancellation. Error probability of higher order bit  $P_{eH}$  is given as a probability that signal  $s_1$  and  $s_2$  exceed threshold  $T_H$ ;

$$\begin{aligned} P_{eH} &= \frac{1}{2} \frac{1}{\sqrt{2\pi\sigma_n}} \left\{ \int_0^{\infty} \exp\left(-\frac{(x + \delta)^2}{2\sigma_n^2}\right) dx \right. \\ &\quad \left. + \int_0^{\infty} \exp\left(-\frac{(x + 3\delta)^2}{2\sigma_n^2}\right) dx \right\}. \end{aligned} \quad (30)$$

Error probability of lower order bit of 16QAM is given as a probability that signal  $s_1$  and  $s_2$  exceed threshold  $T_L$ ;

$$\begin{aligned} P_{eL} &= \frac{1}{2} \frac{1}{\sqrt{2\pi\sigma_n}} \left\{ \int_{-2\delta}^{2\delta} \exp\left(-\frac{(x + 3\delta)^2}{2\sigma_n^2}\right) dx \right. \\ &\quad \left. + \int_{-\infty}^{-2\delta} \exp\left(-\frac{(x + \delta)^2}{2\sigma_n^2}\right) dx \right. \\ &\quad \left. + \int_{2\delta}^{\infty} \exp\left(-\frac{(x + \delta)^2}{2\sigma_n^2}\right) dx \right\}. \end{aligned} \quad (31)$$

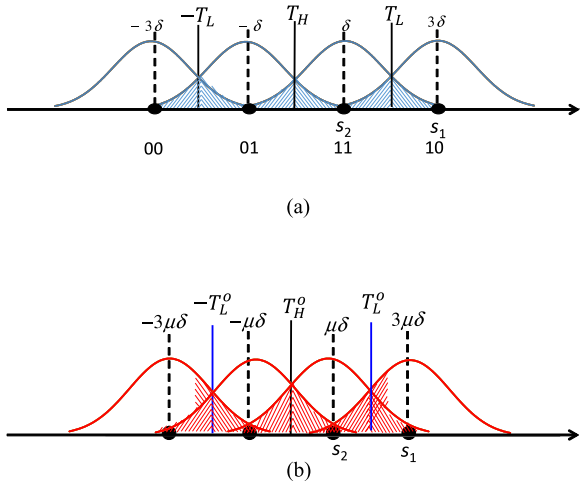


Fig. 6. 16QAM signal distribution (I-phase or Q-phase). (a) w/o peak cancellation (in the presence of AWGN). (b) w/ peak cancellation (in the presence of AWGN and signal distribution).

On the other hand, as illustrated in Fig. 6(b), the average power of the signal and its distribution are reduced by peak cancellation.

Since it is clear that the optimum decision threshold for higher order bit is  $T_H^o = 0$ , error probability of higher order bit is given as

$$\begin{aligned} \hat{P}_{eH}(T_H^o = 0) &= \frac{1}{2} \frac{1}{\sqrt{2\pi(\sigma_n^2 + (\sigma_e^2/\beta))}} \\ &\times \left\{ \int_{T_H^o=0}^{\infty} \exp\left(-\frac{(x + \mu\delta/\sqrt{\beta})^2}{2(\sigma_n^2 + (\sigma_e^2/\beta))}\right) dx \right. \\ &\left. + \int_{T_H^o=0}^{-\infty} \exp\left(-\frac{(x + 3\mu\delta/\sqrt{\beta})^2}{2(\sigma_n^2 + (\sigma_e^2/\beta))}\right) dx \right\}. \end{aligned} \quad (32)$$

Error probability of lower order bit of Gray-coded 16QAM using the optimum decision threshold  $T_L^o$  in AWGN condition in the case with peak cancellation is

$$\begin{aligned} \hat{P}_{eL}(T_L^o) &= \frac{1}{2} \frac{1}{\sqrt{2\pi(\sigma_n^2 + (\sigma_e^2/\beta))}} \\ &\times \left\{ \int_{-T_L^o}^{T_L^o} \exp\left(-\frac{(x + 3\mu\delta/\sqrt{\beta})^2}{2(\sigma_n^2 + (\sigma_e^2/\beta))}\right) dx \right. \\ &+ \int_{-\infty}^{-T_L^o} \exp\left(-\frac{(x + \mu\delta/\sqrt{\beta})^2}{2(\sigma_n^2 + (\sigma_e^2/\beta))}\right) dx \\ &\left. + \int_{T_L^o}^{\infty} \exp\left(-\frac{(x + \mu\delta/\sqrt{\beta})^2}{2(\sigma_n^2 + (\sigma_e^2/\beta))}\right) dx \right\}. \end{aligned} \quad (33)$$

The optimum decision threshold  $T_L^o = -2\mu\delta/\sqrt{\beta}$  to minimize BER can be derived by  $\frac{\partial P_{eL}(T_L^o)}{\partial T_L^o} = 0$ . Details of the derivation are given in the Appendix. Average BER is given by averaging Eq.(32) and Eq.(33).

## B. E-SDM MIMO-OFDM

In this subsection, we consider an Eigen-beam space division multiplexing (E-SDM) OFDM in  $M \times N$  MIMO systems, where  $M$  and  $N$  denotes number of transmit antenna and the number of receive antennas, respectively. Hereafter, we assume  $M = 4$  and  $N = 2$  as an example. PDFs of eigen values with order for random  $M \times N$  MIMO channel matrix are given as [11]:

$$f_1(\lambda) = \Phi_1(\lambda) \exp(-\lambda) + \Phi_2(\lambda) \exp(-2\lambda), \quad (34)$$

$$f_2(\lambda) = -\Phi_1(\lambda) \exp(-2\lambda), \quad (35)$$

where

$$\Phi_1(\lambda) = \lambda^2 \left( \frac{1}{6} \lambda^2 - \lambda + 2 \right),$$

$$\Phi_2(\lambda) = \lambda^2 \left( \frac{1}{6} \lambda^2 + \lambda + 2 \right).$$

Thus, BER expression of signal transmission over the  $i$ -th eigen channels in  $M \times N$  MIMO channel can be derived as

$$P_b^{(i)} = \int_0^{\infty} f_i(\lambda) \left( \int_0^{\infty} p(\lambda, x) dx \right) d\lambda, \quad (36)$$

where  $M$  and  $N$  denote the number of transmit and receive antennas.  $p(\lambda, x)$  denotes PDF of the signal after peak cancellation in presence of AWGN. Similarly single antenna case, for QPSK transmission over  $i$ -th eigen channel,

$$\begin{aligned} p(\lambda, x) &= \frac{1}{\sqrt{2\pi(\sigma_n^2/\lambda + \sigma_e^2 A^2 \lambda)}} \exp \\ &\times \left( -\frac{(x - \bar{x}_e A \sqrt{\lambda} - A)^2}{2(\sigma_e^2 A^2 \lambda + \sigma_n^2/\lambda)} \right). \end{aligned}$$

Average BER over the first and second eigen channel is given as

$$\bar{P}_b = \frac{P_b^{(1)} + P_b^{(2)}}{2}, \quad (37)$$

where the same power is allocated to the first and the second eigen channels.

## VI. PERFORMANCE RESULTS AND DISCUSSIONS

To clarify the validity of the proposed framework, we evaluate the performance of MIMO-OFDM system by computer simulation. The system block diagram is shown in the same as in Fig. 1. We assume QPSK, 16QAM, or 64QAM data modulation. The number of FFT points is 512 and the number of subcarriers is 64. In MIMO cases, Eigen-mode precoding is adopted at each sub-carrier (i.e., E-SDM MIMO), where the transmitter and the receiver equip  $N$  and  $M$  antennas, respectively. The number of streams is denoted as  $K$ . Here, we assume  $K = N$ . Channel model is independent attenuated 6-path Rayleigh fading. The requirement of ACLR is set to  $-50$  dB, while those of EVM are set to  $-20$ ,  $-25$ , and  $-30$  dB for QPSK, 16QAM, and 64QAM cases, respectively. In this paper, we assume that channel estimation is perfectly done at the receiver and channel state information is ideally shared with the transmitter.

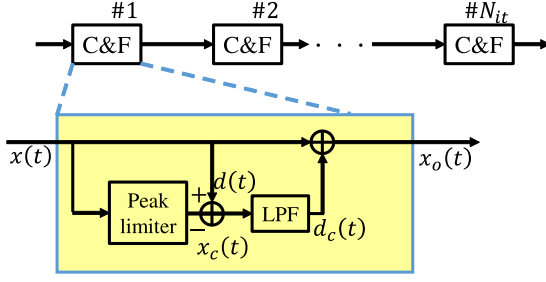


Fig. 7. Block diagram of repeated C&F, where  $N_{it}$  denotes the number of iterations.

One of the conventional approaches is repeated C&F [18], [19]. The block diagram is shown in Fig. 7, where  $x(t)$  and  $x_o(t)$  are the OFDM signals before clipping and after filtering. To reduce the computational complexity, only the clipped signal (i. e., the peak amplitude exceeds a peak detection threshold) is band-limited by filtering operation. Unlike the proposed peak cancellation, this method needs to empirically optimize the filter parameters so as to keep EVM and ACLR values below these pre-defined thresholds.

We also evaluate prior limiter based techniques in [24], [32]. In [24], the peak detection threshold at  $n$ -th iteration  $A_{th}^{(n)}$  in repeated C&F is adaptively determined as

$$A_{th}^{(n)} = \sqrt{\frac{N_f}{N_p}} A_{th}^{(n-1)}, A_{th}^{(0)} = \frac{1}{N_f} \sum_{s=0}^{N_f-1} |x(s\Delta t)|, \quad (38)$$

where  $x(s\Delta t)$  denotes the transmit signal before C&F operation and  $\Delta t$  denotes sampling interval.  $N_f$  and  $N_p$  are the number of FFT points and the number of OFDM samples exceeding  $A_{th}^{(n-1)}$ , respectively. In [32], the following nonlinear function is used to limit peak amplitude:

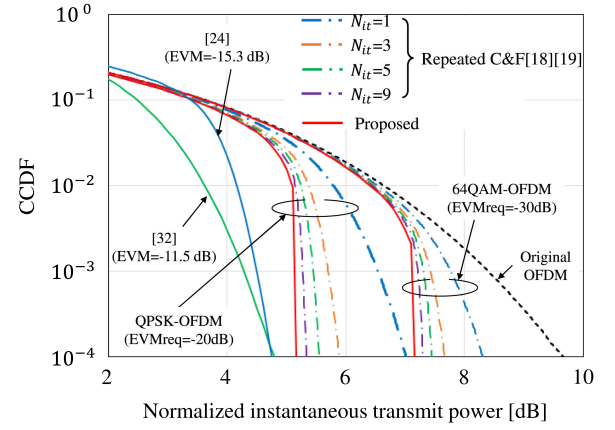
$$y(s\Delta t) = A_{th} \frac{x(s\Delta t)}{|x(s\Delta t)|} \left( 1 + \left( \frac{v}{|x(s\Delta t)|} \right)^{(1/a)} \right)^{-a}, \quad (39)$$

where  $x(s\Delta t)$  and  $y(s\Delta t)$  are input and output complex time-domain signals of the companding function, respectively.  $|x(s\Delta t)|$  denotes the absolute value of  $x(s\Delta t)$ .  $A_{th}$  is the maximum amplitude of  $|y(s\Delta t)|$ .  $v$  and  $a$  are non-linear parameters of the nonlinear function, respectively.

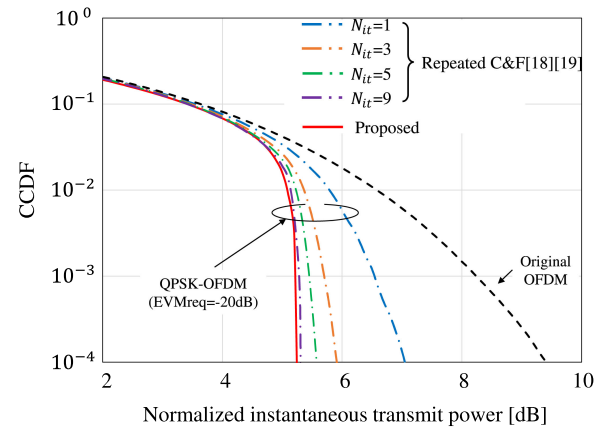
#### A. PAPR

Fig. 8(a) and (b) illustrate the statistical distribution of the normalized instantaneous signal power of transmitting signals in single-antenna OFDM and  $4 \times 2$  MIMO-OFDM, respectively. Here, we use CCDF to evaluate the statistical distribution and the instantaneous is normalized by average power of the signal<sup>1</sup>. For comparison, CCDFs of cases of repeated C&F in [18], [19] and other limiter based approaches in [24], [32] are also shown. In repeated C&F [18], [19], we note here that both ACLR and

<sup>1</sup>Proposed peak cancellation is applicable to MIMO systems with arbitrary number of antennas such as massive MIMO [35]–[38]. Performance analysis of massive MIMO-OFDM with peak cancellation was presented in part in [33].



(a)



(b)

Fig. 8. CCDF of normalized instantaneous transmit power, where  $N_{it}$  denotes the number of iterations in repeated C&F. (a)  $M = N = 1$ . (b)  $M = 4$ ,  $N = 2$ ,  $K = 2$ .

EVM satisfy the required values. In [32],  $v = 7$ ,  $a = 0.05$  and  $A_{th} = 1$  are used. In [24], [32], roll-off filter with roll-off factor = 0 is used. Fig. 8(a) shows that the instantaneous power of transmit signal with the proposed method is limited to around 5.12 dB and 7.25 dB at  $\text{CCDF} = 10^{-4}$  for QPSK and 64QAM data modulation schemes. The optimum threshold values are 55.12 dB and 7.25 dB for QPSK and 64QAM data modulation schemes, respectively. Note that the achieved PAPR by the proposed method is close to the optimum threshold value. In other words, the threshold value corresponds to the achievable PAPR. As for comparison with other approaches, although methods in [24], [32] show lower PAPR than the proposed method, it suffers from high in-band distortion which results in BER degradation as discussed in Fig. 12(b). Note that the proposed method is able to reduce the PAPR to a lower value compared to [24], [32] if the required EVM value is set to a higher value, because the proposed method works to minimize the peak power under given EVM and ACLR requirements. It can be also seen that instantaneous power in the case of repeated C&F is approaching the proposed method by increasing the number of iterations in the repeated C&F; almost the same CCDF in comparison with the proposed method is achieved with



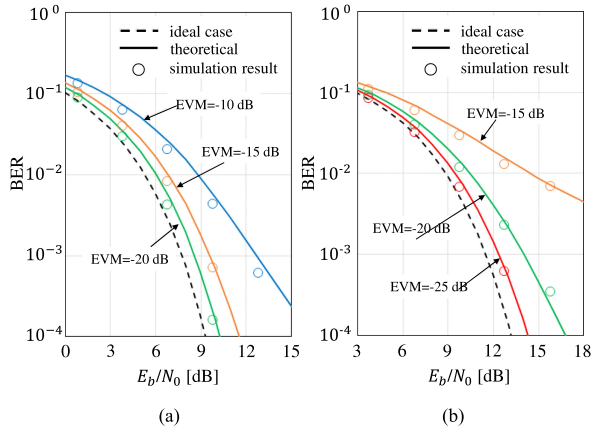


Fig. 9. Theoretical BER performance and its simulation results of OFDM system using the proposed method in AWGN channel. (a) QPSK. (b) 16QAM.

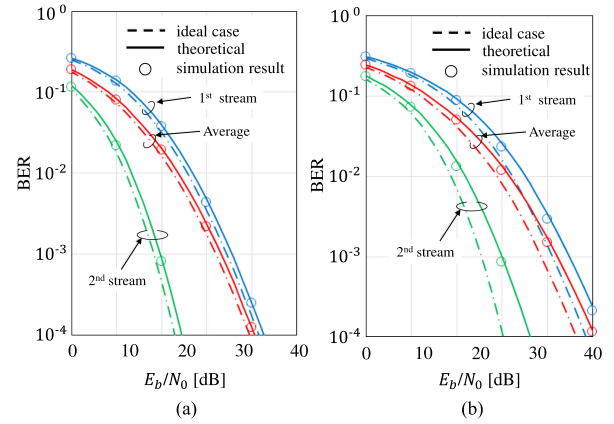


Fig. 11. Theoretical BER and its simulation results of E-SDM OFDM system using the proposed method ( $N = 4$ ,  $M = 2$ ,  $K = 2$ ). (a) QPSK. (b) 16QAM.

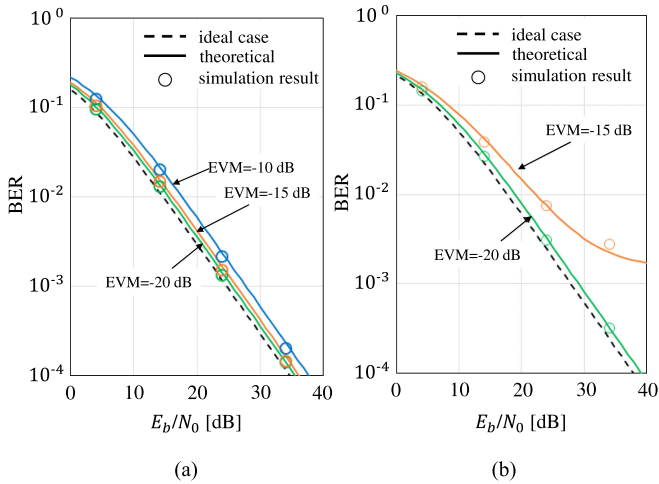


Fig. 10. Theoretical BER performance and its simulation results of OFDM system using the proposed method in Rayleigh fading channel. (a) QPSK. (b) 16QAM.

$N_{it} = 9$ . Similar findings are observed in Fig. 8(b) for E-SDM case.

## B. BER

Fig. 9(a) and (b) illustrate the BER performance of single-antenna OFDM with the peak cancellation in AWGN channel. In this figure, peak cancellation is conducted under ACLR and EVM restrictions. Here, QPSK and 16QAM are used as subcarrier modulation. The BER curve of OFDM without any degradation due to peak cancellation is labeled as “ideal case”. It is demonstrated in Fig. 9(a) that the proposed method achieves very close BER performance to ideal case, where EVM satisfies the pre-defined requirements  $-20$  dB for QPSK and  $-25$  dB for 16QAM, respectively. These figures also indicate that the theoretical BER curves show good agreements with its simulation results.

Figs. 10 and 11 illustrate the BER performance of single-antenna OFDM and  $4 \times 2$  MIMO using eigen-mode in Rayleigh

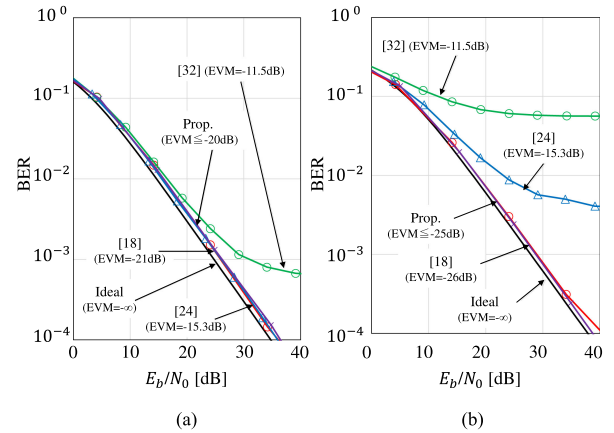


Fig. 12. BER comparison of the proposed method with conventional approaches in Rayleigh fading channel, where QPSK and 16QAM are used as subcarrier modulation, respectively. (a) QPSK. (b) 16QAM.

fading channel, respectively<sup>2</sup>. Here QPSK and 16QAM are used as subcarrier modulation. EVM and ACLR are restricted below the pre-defined values, respectively. These figures also indicate that the theoretical BER curves show good agreements with their simulation results. It can also be seen from Fig. 11 that BER performance of the first and second streams in E-SDM scenarios show good agreements with their simulation results. We note here that EVM and ACLR meet the pre-defined values.

BER of the proposed method is compared with those of the conventional approaches in [18], [24] and [32] in Fig. 12, where QPSK and 16QAM are used for subcarrier modulation in Fig. 12(a) and (b), respectively. The Purple line shows the BER of the repeated C&F [18] using the same threshold as the proposed peak cancellation. The blue line and the green line show the BER of the repeated C&F in [24] and that of the companding technique in [32], respectively. Here, parameters in the repeated C&F and companding are same in Fig. 8(a). The

<sup>2</sup>The proposed framework to analyze theoretical BER performance can be extended to massive MIMO-OFDM with peak cancellation. Details of the BER analysis for massive MIMO-OFDM case is presented in [33].

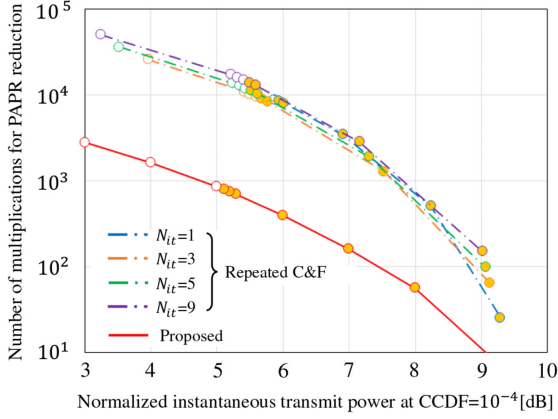


Fig. 13. Number of multiplications per OFDM symbol for PAPR reduction ( $M = 4$ ,  $N = 2$ ,  $K = 2$ ), where QPSK is adopted as subcarrier modulation.

red line shows the BER of the proposed method. In Fig. 12, for QPSK case, it can be seen that the proposed method and conventional methods in [18], [24] show almost the same BER. On the other hand, for 16QAM case, BER of the conventional methods are significantly degraded, while the proposed method shows good BER performance comparable to the ideal case. This is because the proposed method is able to keep EVM below the pre-defined threshold unlike the conventional methods.

### C. Complexity

This subsection evaluates a computational complexity of required PAPR reduction procedures between the two methods above. In this comparison, the number of complex multiplications is used as the complexity metric. When PC signal is added  $N_{pc}$  times per OFDM symbol, the complexity of the proposed method is  $\langle N_w \times N_{pc} \rangle$ , where  $N_w$  denotes the number of complex multiplications per PC addition. On the other hand, the complexity of the C&F with time domain LPF is given as  $\langle \sum_{j=1}^{N_{it}} (N_{tap} \times N_{th}^{(j)}) \rangle$ . Here,  $\langle x \rangle$  denotes the averaging of  $x$ .  $N_{it}$  and  $N_{tap}$  denote the number of iterations and the number of taps in time domain filter, respectively.  $N_{th}^{(j)}$  is the number of samples exceeding a given threshold per OFDM symbol.  $j$  denotes the iteration index.

The required complexity for the peak cancellation in SDM-OFDM is evaluated in comparison with the repeated C&F based on the above defined metric in Fig. 13 where  $M = 4$  and  $N = 2$  are assumed. In the figure, we assume QPSK is adopted as subcarrier modulation. Here, PAPR is defined as the normalized instantaneous power observed at  $CCDF = 10^{-4}$ . The red line shows the result of the proposed method, while the results of repeated C&F method are depicted by other color lines. The color-fill circular shape markers represent that both EVM and ACLR requirements are fulfilled, while the white-fill shows that either EVM or ACLR (or both) exceed the pre-defined value. In repeated C&F cases, normalized instantaneous power is approaching the peak detection threshold  $S_{th} = 10 \log_{10} \frac{A_{th}^2}{S_t}$  by repeating clipping and filtering operations. Note that in the proposed method, ACLR and EVM can be kept below the required

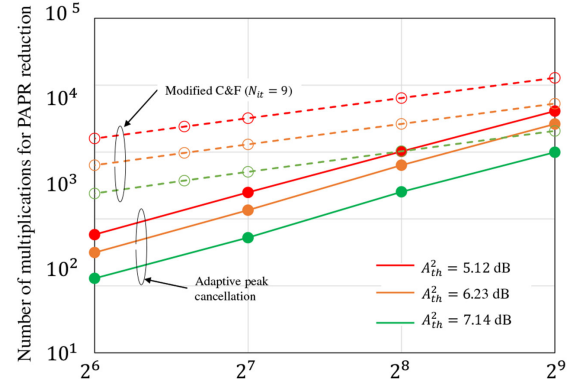


Fig. 14. Relation between the number of subcarriers and the number of multiplications for PAPR reduction.

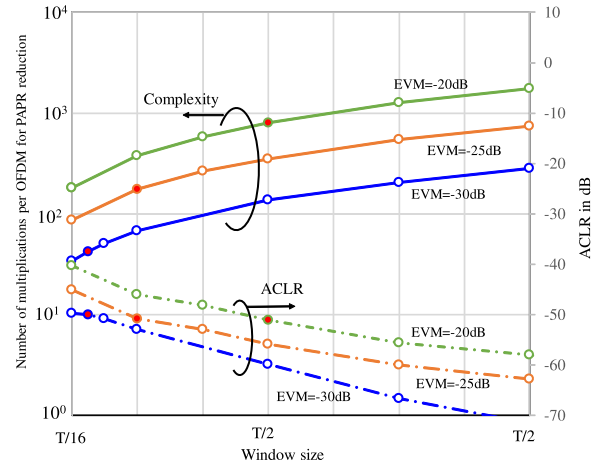


Fig. 15. Relationship between complexity and ACLR in terms of required EVM, where peak detection threshold values are set to optimum values to meet EVM requirements.

values, unlike the repeated C&F method. This figure proves that the required complexity for the proposed peak cancellation is lower in comparison with the repeated C&F.

Fig. 14 show the relation between the number of subcarriers and the number of multiplications for PAPR reduction per antenna, where  $M = 1$  and  $N = 1$  are used. From this figure, we can see that the required complexity increases monotonously as the number of subcarriers increases. It is also clarified that the proposed peak cancellation method achieves lower complexity than modified C&F method in terms of target PAPR value even for case with a large number of antennas. Note that the required complexity per antenna for peak cancellation is the same regardless the number of antennas.

### D. Windowing

Fig. 15 illustrates the relationship between the required complexity and achievable ACLR as a function of window size truncating the PC signal in terms of required EVM values which are set to  $-20$ ,  $-25$  or  $-30$  dB, where red drawn circle markers denote selected window size for each EVM value in case of  $ACLR = -50$  dB. The threshold is selected to meet the required EVM as discussed in Section IV and correspond to achievable

PAPR and BER. The PC signal is truncated by the window function  $w(t)$  as shown by Eqs. (6)–(8). Thus, window-size  $T_2$  affects both ACLR and the complexity. It can be seen that from this figure as window-size increases, ACLR decreases at the expense of increasing the required complexity. The results suggest that the required complexity is minimized by optimizing the window-size under a given EVM (i.e., BER) and threshold value (i.e., PAPR).

## VII. CONCLUSION

Performance analysis of a dynamic peak-cancellation scheme for E-SDM OFDM system has been presented, where EVM and ACLR are restricted below a pre-defined level. Using the proposed approach, degradations due to ACLR and EVM are effectively mitigated while keeping the OoB radiation below its target value. Furthermore, practical design of peak-cancellation signal is discussed with target OoB radiation and in-band distortion through optimizing the windowing size of the PC signal. In addition, we have also theoretically analyzed peak cancellation capability and achieved BER, respectively. Numerical results show that the peak cancellation can improve PAPR of linearly pre-coded E-SDM MIMO-OFDM with low computational complexity. And also, BER performance can be improved by keeping EVM under permissible level at the transmitter side. In addition, we also confirm that theoretical BER show good agreements with simulation results. The proposed peak cancellation approach is applicable to existing methods utilizing degree-of-freedom in massive MIMO systems [35]–[38]. We can expect that the peak cancellation performance can be improved if the transmitter equips a large-scale antenna array that provides extra degree-of-freedom [33], [34]. Detailed analysis of massive MIMO-OFDM with peak cancellation under EVM/ACLR restrictions is our future work.

## APPENDIX

The derivation of  $T_L^o$  in Eq. (33) is as follows. Without loss of generality, we assume  $\beta = 1$ . Since Gray-encoded 16QAM is used, the error probability of lower-order bits is given as

$$\begin{aligned} \hat{P}_{eL}(T_L) &= \frac{1}{2} \frac{1}{\sqrt{2\pi(\sigma_n^2 + \sigma_e^2)}} \\ &\cdot \left\{ \int_{-T_L}^{T_L} \exp\left(-\frac{(x + 3\mu\delta)^2}{2(\sigma_n^2 + \sigma_e^2)}\right) dx \right. \\ &+ \int_{-\infty}^{-T_L} \exp\left(-\frac{(x + \mu\delta)^2}{2(\sigma_n^2 + \sigma_e^2)}\right) dx \\ &\left. + \int_{T_L}^{\infty} \exp\left(-\frac{(x + \mu\delta)^2}{2(\sigma_n^2 + \sigma_e^2)}\right) dx \right\} \\ &= 1 + \operatorname{erf}\left(\frac{T_L + 3\mu\delta}{\sqrt{2(\sigma_n^2 + \sigma_e^2)}}\right) \\ &\quad - \operatorname{erf}\left(\frac{T_L + \mu\delta}{\sqrt{2(\sigma_n^2 + \sigma_e^2)}}\right), \end{aligned} \quad (40)$$

where  $T_L$  is the threshold level to decide I and Q phase of 16QAM constellation points. Using the relationship

$$\int \frac{1}{\sqrt{2\pi\sigma_n^2}} \exp\left(-\frac{x^2}{2\sigma_n^2}\right) dx = \frac{1}{2} \left(1 + \operatorname{erf}\left(\frac{x}{\sqrt{2\sigma_n^2}}\right)\right), \quad (41)$$

the partial differentiation of  $\hat{P}_{eL}(T_L)$  with respect to  $T_L$  is given as

$$\begin{aligned} \frac{\partial \hat{P}_{eL}(T_L)}{\partial T_L} &= \frac{1}{\sqrt{2(\sigma_n^2 + \sigma_e^2)}} \\ &\cdot \left( \exp\left(\frac{(T_L + 3\mu\delta)^2}{2(\sigma_n^2 + \sigma_e^2)}\right) \right. \\ &\quad \left. - \exp\left(\frac{(T_L + \mu\delta)^2}{2(\sigma_n^2 + \sigma_e^2)}\right) \right). \end{aligned} \quad (42)$$

By solving  $\frac{\partial \hat{P}_{eL}(T_L^o)}{\partial T_L^o} = 0$ ,

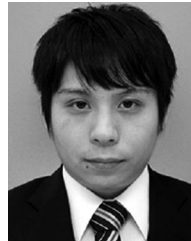
$$\begin{aligned} \exp\left(\frac{(T_L^o + 3\mu\delta)^2}{2(\sigma_n^2 + \sigma_e^2)}\right) &= \exp\left(\frac{(T_L^o + \mu\delta)^2}{2(\sigma_n^2 + \sigma_e^2)}\right) \\ (T_L^o + 3\mu\delta)^2 &= (T_L^o + \mu\delta)^2 \\ T_L^o &= -2\mu\delta, \end{aligned} \quad (43)$$

where  $-2\mu\delta$  is an intersection point of two Gaussian distributions located on the left side of the horizontal axis of 16QAM constellation as shown in Fig. 6(b).

## REFERENCES

- [1] T. Hwang, C. Yang, G. Wu, S. Li, and G. Ye Li, "OFDM and its wireless applications: A Survey," *IEEE Trans. Veh. Tech.*, vol. 58, no. 4, pp. 1673–1694, May 2009.
- [2] Y. Akaiwa, *Introduction to Digital Mobile Communication*. 2nd Edition, Hoboken, NJ, USA: Wiley, Jun. 2015.
- [3] S. H. Han and J. H. Lee, "An overview of peak-to-average power ratio reduction techniques for multicarrier transmission," *IEEE Wireless Commun.*, vol. 12, no. 2, pp. 56–65, Apr. 2005.
- [4] Y. Rahmatallah and S. Mohan, "Peak-to-average power ratio reduction in OFDM systems: A survey and taxonomy," *IEEE Commun. Surv. Tut.*, vol. 15, no. 4, pp. 1567–1592, Oct.–Dec. 2013.
- [5] R. W. Bauml, R. F. H. Fischer, and J. B. Huber, "Reducing the peak-to-average power ratio of multicarrier modulation by selected mapping," *Electron. Lett.*, vol. 32, no. 22, pp. 2056–2057, Oct. 1996.
- [6] D.-W. Lim, J.-S. No, C.-W. Lim, and H. Chung, "A new SLM OFDM scheme with low complexity for PAPR reduction," *IEEE Signal Process. Lett.*, vol. 12, no. 2, pp. 93–96, Feb. 2005.
- [7] S. H. Müller and J. B. Huber, "OFDM with reduced peak-to-average power ratio by optimum combination of partial transmit sequence," *Electron. Lett.*, vol. 33, no. 5, pp. 368–369, Feb. 1997.
- [8] L. J. Cimini and N. R. Sollenberger, "Peak-to-average power ratio reduction of an OFDM signal using partial transmit sequence," *IEEE Commun. Lett.*, vol. 4, no. 3, pp. 86–88, Mar. 2000.
- [9] O. Muta and Y. Akaiwa, "Weighting factor estimation method for peak power reduction based on adaptive flipping of parity bits in turbo-coded OFDM systems," *IEEE Trans. Veh. Technol.*, vol. 57, no. 6, pp. 3551–3562, Nov. 2008.
- [10] O. Muta, "Construction and blind estimation of phase sequences for subcarrier-phase control based PAPR reduction in LDPC-Coded OFDM systems," *IEICE Trans. Fundam.*, vol. E93-A, no. 11, pp. 2130–2140, Nov. 2010.

- [11] J. Tellado and J. M. Cioffi, "Efficient algorithms for reducing PAR in multicarrier systems," in *Proc. IEEE Int. Symp. Inf. Theory*, Aug. 1998, p. 191.
- [12] P. Boonsrimuang, K. Mori, T. Paungma, and H. Kobayashi, "Proposal of simple PAPR reduction method for OFDM signal by using dummy sub-carriers," *IEICE Trans. Commun.*, vol. E91.B, no. 3, pp. 784–794, Mar. 2010.
- [13] B. S. Krongold and D. L. Jones, "PAR reduction in OFDM via active constellation extension," *IEEE Trans. Broadcast.*, vol. 49, no. 3, pp. 258–268, Sep. 2003.
- [14] T. A. Wilkinson, and A. E. Jones, "Minimization of the peak to mean envelope power ratio of multicarrier transmission schemes by block coding," in *Proc. IEEE Veh. Technol. Conf.*, 1995, pp. 825–829.
- [15] A. E. Jones and T. A. Wilkinson, "Combined coding for error control and increased robustness to system nonlinearities in OFDM," in *Proc. IEEE Veh. Technol. Conf.*, 1996, pp. 904–908.
- [16] S. Shepherd, J. Orriss, and S. Barton, "Asymptotic limits in peak envelope power reduction by redundant coding in orthogonal frequency-division multiplex modulation," *IEEE Trans. Commun.*, vol. 45, no. 1, pp. 5–10, Jan. 1998.
- [17] X. Li and L. J. Cimini, "Effect of clipping and filtering on the performance of OFDM," *IEEE Commun. Lett.*, vol. 2, no. 5, pp. 131–133, May 1998.
- [18] J. Armstrong, "Peak-to-average power reduction for OFDM by repeated clipping and frequency domain filtering," *Electron. Lett.*, vol. 38, no. 5, pp. 246–247, Feb. 2002.
- [19] S. Tomisato and H. Suzuki, "A peak reduction scheme based on control signal insertion for multi-carrier mobile communication," *IEICE Trans. Commun.*, vol. E86-B, no. 6, pp. 1910–1916, Jun. 2003.
- [20] M. M. Lee and Y. Kim, "An adaptive clipping and filtering technique for PAPR reduction in OFDM systems," *Circuits Syst. Signal Process.* vol. 32, no. 3, pp. 1335–1349, Jun. 2013.
- [21] Y.-C. Wang and A.-Q. Luo, "Optimized iterative clipping and filtering for PAPR reduction of OFDM signals," *IEEE Trans. Commun.*, vol. 59, no. 1, pp. 33–37, Jan. 2011.
- [22] X. Zhu, W. Pan, H. Li, and Y. Tang, "Simplified approach to optimized iterative clipping and filter for PAPR reduction of OFDM signals," *IEEE Trans. Commun.*, vol. 61, no. 5, pp. 1891–1901, May 2013.
- [23] I. Sohn and S. C. Kim, "Neural network based simplified clipping and filtering technique for PAPR reduction of OFDM signals," *IEEE Commun. Lett.*, vol. 19, no. 8, pp. 1438–1441, Aug. 2015.
- [24] K. Anoh, C. Tanriover, B. Adebisi, and M. Hammoudeh, "A new approach to iterative clipping and filtering PAPR reduction scheme for OFDM systems," *IEEE Access*, vol. 6, pp. 17533–17544, Sep. 2017.
- [25] M. Pauli and H.-P. Kuchenbecker, "Minimization of the intermodulation distortion of a nonlinearly amplified OFDM signal," *Wireless Personal Commun.*, vol. 4 pp. 93–101, 1996.
- [26] X. Huang, J. Lu, J. Zheng, K. B. Letaief, and J. Gu, "Companding transform for reduction in peak-to-average power ratio of OFDM signals," *IEEE Trans. Wireless Commun.*, vol. 3, no. 6, pp. 2030–2039, Nov. 2004.
- [27] T. Jiang, Y. Yang, and Y. Song, "Exponential companding technique for PAPR reduction in OFDM systems," *IEEE Trans. Broadcast.*, vol. 51, no. 2, pp. 244–248, Jun. 2005.
- [28] L. Dan, T. Li, Y. Xiao, and S. Li, "Performance of peak cancellation for PAPR reduction in OFDM system," in *Proc. Int. Conf. Commun., Circuits Syst.*, 2008, pp.283–287.
- [29] Y. Huang, "A simplified peak cancellation method for OFDM signals," in *Proc. Int. Conf. Comput. Sci. Electron. Eng.*, 2012, pp. 336–339.
- [30] T. Hino, O. Muta, and H. Furukawa, "A study on peak amplitude suppression of OFDM signals under restriction of out-of-band radiation power," *Trans. IEICE B*, vol. J97-B, no. 6, pp. 271–275, Jun. 2014 (in Japanese).
- [31] T. Kageyama, O. Muta, and H. Gacanin, "An adaptive peak cancellation method for linear pre-coded MIMO-OFDM signals," in *Proc. Annu. IEEE Int. Symp. Personal, Indoor Mobile Radio Commun.*, Sep. 2015.
- [32] B. Adebisi, K. Anoh, and K. M. Rabie, "Enhanced nonlinear companding scheme for reducing PAPR of OFDM systems," *IEEE Syst. J.*, vol. 13, no. 1, pp. 65–75, Mar. 2019.
- [33] T. Kageyama and O. Muta, "Bit error analysis of MRC pre-coded massive MIMO-OFDM systems with peak cancellation," in *Proc. IEEE 90th Veh. Technol. Conf.*, Sep. 2019.
- [34] T. Kageyama, O. Muta, C. M. Chen, and S. Pollin, "Effect of limiter based PAPR reduction for massive MIMO-OFDM," in *Proc. Int. Japan-Africa Conf. Electron., Commun. Computations*, Dec. 2018, pp. 43–46.
- [35] M. Yao, M. Carrick, M. M. Sohal, V. Marojevic, C. D. Patterson, and J. H. Reed, "Semidefinite relaxation-based PAPR-aware precoding for massive MIMO-OFDM systems," *IEEE Trans. Veh. Tech.*, vol. 68, no. 3, pp. 2229–2243, Mar. 2019.
- [36] C. Studer and E. G. Larsson, "PAR-aware large-scale multi-user MIMO-OFDM downlink," *IEEE J. Sel. Areas Commun.*, vol. 31, no. 2, pp. 303–313, Feb. 2013.
- [37] H. Bao, J. Fang, Q. Wan, Z. Chen, and T. Jiang, "An ADMM approach for PAPR reduction for large-scale MIMO-OFDM systems," *IEEE Trans. Veh. Tech.*, vol. 67, no. 8, Aug. 2018, pp. 7407–7418.
- [38] R. Zayani, H. Shaiek, and D. Roviras, "PAPR-aware massive MIMO-OFDM downlink," *IEEE Access*, vol. 7, pp. 25474–25484, Feb. 2019.



**Tomoya Kageyama** (Student Member, IEEE) received the B.E. and M.E. degrees, in 2015 and 2017, respectively, from Kyushu University, Fukuoka, Japan, where he is currently working toward the doctoral degree. His research interests include PHY layer signal processing techniques for powerline communications and MIMO wireless communications.



**Osamu Muta** (Member, IEEE) received the B.E. degree from Ehime University, Matsuyama, Japan, in 1996, the M.E. degree from the Kyushu Institute of Technology, Kitakyushu, Japan, in 1998, and the Ph.D. degree from Kyushu University, Fukuoka, Japan, in 2001. In 2001, he joined the Graduate School of Information Science and Electrical Engineering, Kyushu University as an Assistant Professor. Since 2010, he has been an Associate Professor with the Center for Japan-Egypt Cooperation in Science and Technology, Kyushu University. His current research interests include signal processing techniques for wireless communications and powerline communications, interference coordination techniques, MIMO, and nonlinear distortion compensation techniques for high-power amplifiers. He is a Senior Member of the Institute of Electronics, Information, and Communication Engineering (IEICE). He is the recipient of the 2005 Active Research Award from IEICE technical committee of radio communication systems, and Chairman's (Best Paper) Award from IEICE Technical Committee of Communication Systems (2014, 2015, and 2017).



**Haris Gacanin** (Senior Member, IEEE) received the Dipl.-Ing. degree in electrical engineering from the University of Sarajevo, Sarajevo, Bosnia and Herzegovina, in 2000. He received the M.Sc. and Ph.D. degrees from Tohoku University, Sendai, Japan, in 2005 and 2008, respectively. He was with Tohoku University from 2008 until 2010 first as Japan Society for Promotion of Science Postdoctoral Fellow and later, as an Assistant Professor. He joined Alcatel-Lucent (now Nokia) in 2010, where he worked as Physical-layer Expert, Research Director, and the

Department Head with Nokia Bell Labs until 2020. During 2018–2020, he was an Adjunct Professor with the University of Leuven, Leuven, Belgium. He is currently a Full (Chair) Professor with RWTH Aachen University, Aachen, Germany. He has authored 200+ scientific publications (journals, conferences, and patent applications) and invited/tutorial talks. His professional interests are related to broad areas of digital signal processing and artificial intelligence with applications in communication systems. He is a Distinguished Lecturer of IEEE Vehicular Technology Society and an Associate Editor for the IEEE Communications Magazine, while he was an Editor for the *IEICE Transactions on Communications* and *IET Communications*. He is Senior Member of the Institute of Electronics, Information and Communication Engineering (IEICE) and acted as the General Chair and Technical Program Committee Member of various IEEE conferences. He is the recipient of several Nokia innovation awards, IEICE Communication System Study Group Best Paper Award (joint 2014, 2015, 2017), The 2013 Alcatel-Lucent Award of Excellence, the 2012 KDDI Foundation Research Award, the 2009 KDDI Foundation Research Grant Award, the 2008 Japan Society for Promotion of Science (JSPS) Postdoctoral Fellowships for Foreign Researchers, the 2005 Active Research Award in Radio Communications, 2005 Vehicular Technology Conference (VTC 2005-Fall) Student Paper Award from IEEE VTS Japan Chapter and the 2004 Institute of IEICE Society Young Researcher Award. He was awarded by Japanese Government (MEXT) Research Scholarship in 2002.